Sparse Approximation of an Outdoor-to-Indoor Massive MIMO Channel Measurement

Herbert Groll*, Daniel Schützenhöfer*†, Stefan Pratschner*†, Peter Gerstoft‡, Christoph F. Mecklenbräuker*

* Institute of Telecommunications, TU Wien, Austria, *herbert.groll@tuwien.ac.at*
† Christian Doppler Laboratory for Dependable Wireless Connectivity for the Society in Motion
‡ University of California San Diego

***Abstract*—Models for the wireless channel for massive multiple-input multiple-output (MIMO) communication in the sub-6 GHz frequencies often assume a rich scattering environment. However, measurements in outdoor-to-indoor scenarios indicate a low rank of the wireless channel coefficients matrix. We approximate a measured 70x169 massive MIMO outdoor-to-indoor channel with its sparse representation by applying atomic norm minimization. We further investigate the enhanced resolution in direction of departure and direction of arrival for closely located multipath components compared to conventional beamforming. Finally, we compare the achievable rate for the measured channel with sparse approximated versions.**

***Index Terms*—atomic norm minimization, sparse approximation, massive mimo, double directional**

I. Introduction

Massive multiple-input multiple-output (MIMO) in wireless communications is a multi user technique which enhances the spectral efficiency by employing many antennas at the base stations [1]. Acquiring accurate channel state information is a crucial task for transmit precoding in massive MIMO. Further, high angular resolution of antenna arrays and a rich scattering environment are both important to enable good user separability and to increase the performance [2]. Some scenarios lack diffuse and specular components due to the absence of scattering objects which leads to a low rank of the MIMO channel coefficients matrix. In those cases, high resolution techniques are essential to maintain user separability.

We analyze a measured 70x169 massive MIMO outdoor-to-indoor wireless channel within the framework of atomic norm minimization with respect to approximation performance and achievable angular resolution. The MIMO channel measurement data is from a virtual array measurement campaign [3] in an static scenario as shown in Fig. 1. A transmit array (TX) is located outdoor on an roof. A receive array (RX) is located indoor at 150 m distance.

For the analysis of the gathered wireless MIMO channel estimate, the atomic norm allows the sparse presentation of a signal by atoms from an infinite-dimensional set [5]. Atomic norm minimization (ANM) is a popular technique for gridless sparse frequency estimation [6], [7]. Furthermore, in [8] it was shown, that atomic norm minimization is equivalent to the mixed gridless $\ell_{2,1}$ norm minimization problem.

For direction of arrival (DOA) estimation, those frequencies are spatial frequencies. Finding the atomic norm with a convex relaxation is the continuous counterpart to the ℓ_1 norm in sparse vector recovery [6]. This leads to a computationally efficient semi-definite program (SDP) to find a sparse representation [6].

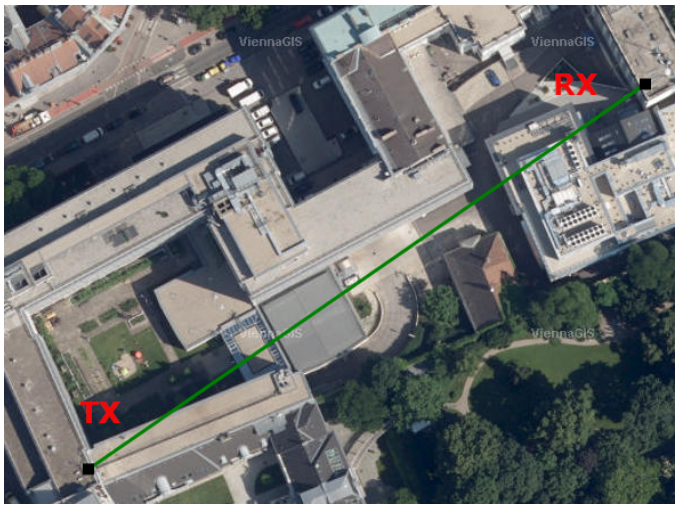

Fig. 1. Aerial photo [4] of the MIMO measurement. The transmit array is on a rooftop. The receive array is inside an office.

II. Method

The virtual MIMO measurement consists of NM individual measurements between N transmit and M receive antenna elements. The p-th receive vector $\mathbf{y}_p \in \mathbb{C}^M$ is

$$\mathbf{y}_p = \mathbf{H}\mathbf{e}_\mathbf{p} s_p + \mathbf{w}_p, \tag{1}$$

where $\mathbf{H} \in \mathbb{C}^{M\times N}$ is the full MIMO channel matrix, $\mathbf{e_p}$ is the TX antenna selecting vector with 1 at position p and 0 elsewhere, the unitary transmit amplitude $s_p = 1 \forall p \in \{1, \dots, N\}$, and $\mathbf{w}_p$ is additive white Gaussian noise. The full measurement is collected in $\mathbf{Y} = [\mathbf{y}_1 \mathbf{y}_2 \dots \mathbf{y}_N] \in \mathbb{C}^{M\times N}$ as

$$\mathbf{Y} = \mathbf{H}[\mathbf{e_1}\mathbf{e_2}\dots\mathbf{e_N}]s + \mathbf{W} = \mathbf{H}s + \mathbf{W}. \tag{2}$$

With a narrowband plane-wave assumptions, the fully-directional MIMO channel matrix $\mathbf{H}$ is a sum of L discrete paths with transmit and receive steering responses [9]

$$\mathbf{H} = \mathbf{B}(\mathbf{f}_B)\mathbf{D}\mathbf{A}^H(\mathbf{f}_A) = \sum_{l=1}^{L} \alpha_l \mathbf{b}(\mathbf{f}_{b,l})\mathbf{a}^H(\mathbf{f}_{a,l}) \ , \tag{3}$$

where $(\,)^H$ denotes the conjugate-transpose, $\mathbf{B}(\mathbf{f}_B)$ is the steering matrix with steering response vectors for all RX antenna elements as columns $\mathbf{b}(\mathbf{f}_{b,l})$, $\mathbf{A}(\mathbf{f}_A)$ is the steering matrix with steering response vectors for all TX antenna elements as columns $\mathbf{a}(\mathbf{f}_{a,l})$, α_l is the complex gain for path l, and $\mathbf{D} = \mathrm{diag}([\alpha_1, \ldots, \alpha_L])$.

For a uniform planar array (UPA) with $\lambda/2$ spacing, the array responses can be factorized as [10, sec. 4.1.2]

$$\mathbf{c}_I(\mathbf{f}) = \mathbf{c}_{I_1}(f_1) \otimes \mathbf{c}_{I_2}(f_2) \in \mathbb{C}^{I_1 I_2}\ , \tag{4}$$

$$\mathbf{c}_{I_i}(\mathbf{f}) = [\mathrm{e}^{j2\pi(0)f_i},\ \ldots\ , \mathrm{e}^{j2\pi(I_i-1)f_i}]^T\ , i \in \{1, 2\} \tag{5}$$

where $\otimes$ denotes the Kronecker product, I_i is number of elements in direction i, and $\mathbf{f} = [f_1, f_2]^T$ are the spatial frequencies with $f_i \in [0, 1)$. For the transmitter $\mathbf{a}(\mathbf{f}_a) = \mathbf{c}_{N_1}(f_{a_1}) \otimes \mathbf{c}_{N_2}(f_{a_2})$ and for the receiver $\mathbf{b}(\mathbf{f}_b) = \mathbf{c}_{M_1}(f_{b_1}) \otimes \mathbf{c}_{M_2}(f_{b_2})$.

The vectorization of (3) with (4) allows a formulation of the full MIMO channel matrix $\mathbf{h} = \mathrm{vec}(\mathbf{H})$, i.e. the columns of $\mathbf{H}$ stacked into a vector, as a sum of four-dimensional complex sinusoids

$$\mathbf{h} = \sum_l \alpha_l \mathbf{c}^*_{N_1}(f_{a_1,l}) \otimes \mathbf{c}^*_{N_2}(f_{a_2,l}) \otimes \mathbf{c}_{M_1}(f_{b_1,l}) \otimes \mathbf{c}_{M_2}(f_{b_2,l}). \tag{6}$$

The sum is composed out of atoms from the continuous atomic set $\mathcal{A}$, defined as

$$\mathcal{A} = \{\mathbf{a}^*(\mathbf{f}_a) \otimes \mathbf{b}(\mathbf{f}_b)\ :\ \mathbf{f}_a \in [0, 1)^2, \mathbf{f}_b \in [0, 1)^2\}, \tag{7}$$

where $[0, 1)^2 = [0, 1) \times [0, 1)^2$. The framework of atomic norm minimization helps in finding the sparsest representation of $\mathbf{h}$ in $\mathcal{A}$, where the atomic norm has the following equivalent form for four-dimensional complex sinusoids [5], [11]

$$\|\mathbf{h}\|_{\mathcal{A}} = \inf\Bigg\{ \frac{1}{2MN}\mathrm{Tr}\left(\mathbf{T}_4(\mathbf{u})\right) + \frac{1}{2}t : \begin{bmatrix} \mathbf{T}_4(\mathbf{u}) & \mathbf{h} \\ \mathbf{h}^H & t \end{bmatrix} \succeq 0, t > 0 \Bigg\}, \tag{8}$$

where $\mathbf{T}_4(\mathbf{u}) \in \mathbb{C}^{MN \times MN}$ is a positive semi-definite (PSD) four-level Toeplitz-block-Toeplitz matrix and the vector $\mathbf{u} = [u_1 \ldots u_n] \in \mathbb{C}^n$, with $n = (2M_1 - 1)(2M_2 - 1)(2N_1 - 1)(2N_2 - 1)$, fully parameterizes $\mathbf{T}_4(\mathbf{u})$. At the d-th level, $\mathbf{T}_d$ is block-Toeplitz with blocks of $(d-1)$-level Toeplitz-block-Toeplitz matrices $\mathbf{T}_{d-1}$ and so on. For information on construction c.f. [9], [11]. For $d = 1$, $\mathbf{T}_1 \in \mathbb{C}^{N_2 \times N_2}$ is Toeplitz with $(2N_2 - 1)$ variables. Frequencies can be recovered from $\mathbf{T}_4(\mathbf{u})$ with multi-level Vandermonde decomposition, e.g. with matrix pencil and auto-pairing (MAPP) [11]. The resulting frequencies are from a continuum, i.e. gridless, and correspond to TX and RX steering vectors of distinct paths.

Solving (8) is possible with a SDP but still of high computational complexity. To reduce complexity, we decompose the atoms of $\mathbf{H}$ into two decoupled two-dimensional atoms in a multiple measurement vector (MMV) scenario [6], [9], [12], i.e., each transmit antenna position produces a single snapshot. We introduce the set of matrix atoms as

$$\mathcal{A}_M = \{\mathbf{b}(\mathbf{f}_b)\mathbf{a}^H(\mathbf{f}_a)\ :\ \mathbf{f}_a \in [0, 1)^2, \mathbf{f}_b \in [0, 1)^2\}. \tag{9}$$

The atomic norm corresponding to $\mathcal{A}_M$ is

$$\|\mathbf{H}\|_{\mathcal{A}_M} = \inf_{\substack{\mathbf{f}_a \in [0,1)^2, \\ \mathbf{f}_b \in [0,1)^2}} \left\{ \sum_l |\alpha_l| \;\middle|\; \mathbf{H} = \sum_l \alpha_l \mathbf{b}(\mathbf{f}_b, l)\mathbf{a}^H(\mathbf{f}_a, l) \right\}, \tag{10}$$

where the atoms are in matrix form and $\mathbf{H}$ composed out of rank-one matrices. If the spatial frequencies are sufficiently separated, a decoupled version of the equivalent form of (10) is [9]

$$\|\mathbf{H}\|_{\mathcal{A}_M} = \inf_{\substack{\mathbf{f}_a \in [0,1)^2, \\ \mathbf{f}_b \in [0,1)^2}} \Bigg\{ \frac{1}{2M}\mathrm{Tr}\left(\mathbf{T}_2(\mathbf{u})\right) + \frac{1}{2N}\mathrm{Tr}\left(\mathbf{T}_2(\mathbf{v})\right) : \begin{bmatrix} \mathbf{T}_2(\mathbf{v}) & \mathbf{H}^H \\ \mathbf{H} & \mathbf{T}_2(\mathbf{u}) \end{bmatrix} \succeq 0 \Bigg\}. \tag{11}$$

We can not guarantee sufficient frequency separation in the outdoor-to-indoor scenario. An approximate attempt to solve for $\mathcal{A}_M$ is done with the following SDP [9]

$$\min_{\substack{\hat{\mathbf{H}}, \\ \mathbf{u}, \\ \mathbf{v}}} . \quad \frac{\mu}{2M}\mathrm{Tr}\left(\mathbf{T}_2(\mathbf{u})\right) + \frac{\mu}{2N}\mathrm{Tr}\left(\mathbf{T}_2(\mathbf{v})\right) + \frac{1}{2}\|\hat{\mathbf{H}} - \mathbf{H}\|_F^2$$
$$\text{s.t.} \begin{bmatrix} \mathbf{T}_2(\mathbf{v}) & \hat{\mathbf{H}}^H \\ \hat{\mathbf{H}} & \mathbf{T}_2(\mathbf{u}) \end{bmatrix} \succeq 0, \tag{12}$$

where $\mathbf{u} \in \mathbb{C}^{(2M_1-1)(2M_2-1)}$ and $\mathbf{v} \in \mathbb{C}^{(2N_1-1)(2N_2-1)}$ parameterize the corresponding two-level Toeplitz matrices $\mathbf{T}_2(\mathbf{u})$ and $\mathbf{T}_2(\mathbf{v})$, and $\hat{\mathbf{H}}$ is the approximated matrix. In the presence of noise, this minimization problem needs to regularize between Toeplitz structure and the assumed Gaussian noise via a regularization parameter μ.

The approximated channel matrix $\hat{\mathbf{H}}$ does not have a sparse representation. We extract an estimate of K spatial frequencies $\tilde{\mathbf{f}}_A$ and $\tilde{\mathbf{f}}_B$ by applying the two-dimensional MAPP method on $\mathbf{T}_2(\mathbf{v})$ and $\mathbf{T}_2(\mathbf{u})$. The Toeplitz matrices allow the decompositions

$$\mathbf{T}_2(\mathbf{v}) = \mathbf{A}(\tilde{\mathbf{f}}_A)\mathbf{D}_V\mathbf{A}^H(\tilde{\mathbf{f}}_A), \tag{13}$$

$$\mathbf{T}_2(\mathbf{u}) = \mathbf{B}(\tilde{\mathbf{f}}_B)\mathbf{D}_U\mathbf{B}^H(\tilde{\mathbf{f}}_B). \tag{14}$$

An frequency pairing step is necessary between $\hat{\mathbf{f}}_a$ and $\hat{\mathbf{f}}_b$ with an extension to the pairing algorithm in [13]. The array response matrices $\mathbf{A}(\hat{\mathbf{f}}_A)$ and $\mathbf{B}(\hat{\mathbf{f}}_B)$ for TX and RX, respectively, correspond to K different paths which are still decoupled between TX and RX. First, we recover $\mathbf{D}$ from (3) with

$$\hat{\mathbf{D}} = \mathbf{B}(\hat{\mathbf{f}}_B)^+\hat{\mathbf{H}}\left(\mathbf{A}^H(\hat{\mathbf{f}}_A)\right)^+, \tag{15}$$

where $(\,)^+$ denotes the pseudo-inverse. Second, from (14) we recover the diagonal matrix $\mathbf{D}_U$. Third, frequencies $\hat{\mathbf{f}}_{b,i}$ and $\hat{\mathbf{f}}_{a,j}$ are paired if $|\mathbf{D}_U^{-1}\hat{\mathbf{D}}| \geq \varepsilon_f$ and reordered as $\tilde{\mathbf{f}}_B$ and $\hat{\mathbf{f}}_A$.

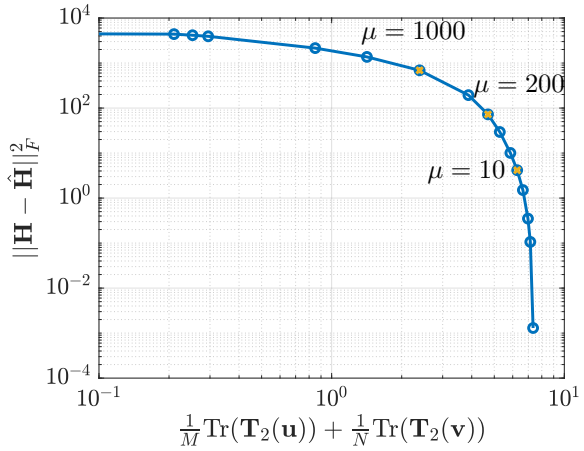

Fig. 2. Optimal trade-off curve between sparsity and quality of measurement reconstruction.

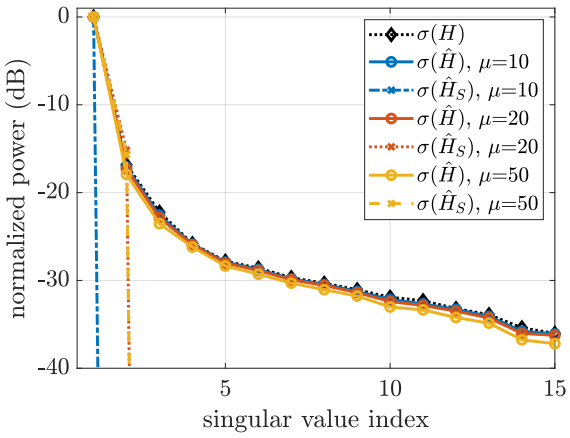

Fig. 3. Power of squared singular values σ of measured $\mathbf{H}$, approximated $\hat{\mathbf{H}}$, and approximated sparse $\hat{\mathbf{H}}_S$ channel matrices. Normalized to maximum singular value.

Path gains are extracted from $\hat{\mathbf{H}}$ similar to (15) with paired frequencies as in [14] with

$$\tilde{\mathbf{D}} = \mathbf{B}(\tilde{\mathbf{f}}_B)^{+}\hat{\mathbf{H}}\left(\mathbf{A}^H(\tilde{\mathbf{f}}_A)\right)^{+}, \tag{16}$$

with the diagonals as vector $\tilde{\alpha} = [\tilde{\alpha}_1, \ldots, \tilde{\alpha}_K]^T = \mathrm{diag}(\tilde{D})$, which then allows a sparse representation as

$$\hat{\mathbf{H}}_S = \sum_{l=1}^{K} \tilde{\alpha}\mathbf{b}(\tilde{\mathbf{f}}_{b,l})\mathbf{a}^H(\tilde{\mathbf{f}}_{a,l}), \tag{17}$$

with its parameters $\tilde{\mathbf{f}}_A \in [0,1)^{2\times K}$, $\tilde{\mathbf{f}}_B \in [0,1)^{2\times K}$, and $\tilde{\alpha} \in \mathbb{C}^K$.

III. Results

The MIMO channel measurement data is from a virtual array measurement campaign [3] shown in Fig. 1. The virtual array is composed of $N = 70$ ($N_1 = 10$ and $N_2 = 7$) transmit antennas with $\lambda/2$ spacing in the $z-y$ plane, and $M = 169$ ($M_1 = 13$ and $M_2 = 13$) receive antennas with $\lambda/2$ spacing in the $x-y$ plane.

The measurement matrix $\mathbf{H}$ is normalized to $\|\mathbf{H}\|_F^2 = MN$. For evaluation $K = 5$ and $\varepsilon_f = 0.2$.

A. Optimal Trade-Off Curve

The SDP in (12) involves a parameter μ to tune between sparsity of the approximated matrix $\hat{\mathbf{H}}$ and quality of reconstruction determined via the squared Frobenius norm of the reconstruction error. Fig. 2 shows the optimal trade-off curve on a logarithmic scale. The convex solver does not find a solution below $\mu = 0.1$, as the Toeplitz structure constraint is too strict. A trade-off is achieved, e.g. with $\mu \in [10, 1000]$ before the reconstruction error starts to saturate with further increasing μ.

The singular values of the measured, the approximated, and the approximated sparse channel matrices for different μ are shown in Fig. 3. The number of singular values with high power is decreasing for $\sigma(\hat{\mathbf{H}})$ with increasing μ. Only one singular value of $\sigma(\hat{\mathbf{H}}_S)$ is within the dynamic range.

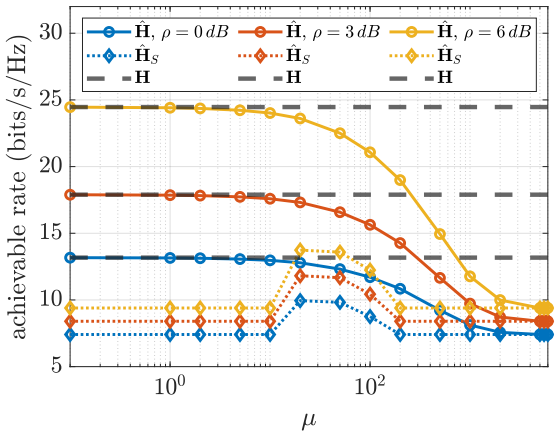

Fig. 4. Achievable rate of the measured MIMO channel compared to the approximated channel for different signal to noise ratios ρ.

B. Achievable Rate

The achievable rate of the approximation of the channel is compared to the measured channel, as shown in Fig. 4, is defined as

$$C_i = \log_2 \det\left(\mathbf{I}_{M_1 M_2} + \frac{\rho}{N_1 N_2}\mathbf{H}_i\mathbf{H}_i^H\right) \tag{18}$$

where ρ is the averaged signal-to-noise ratio (SNR), C_i corresponds to the measured ($i = 1$), to the approximated ($i = 2$), and to the approximated sparse ($i = 3$) channel matrix. The achievable rate of $\sigma(\hat{\mathbf{H}})$ is upper bounded by the rate of $\sigma(\mathbf{H})$ and lower bounded by the rate of $\sigma(\hat{\mathbf{H}}_S)$. The

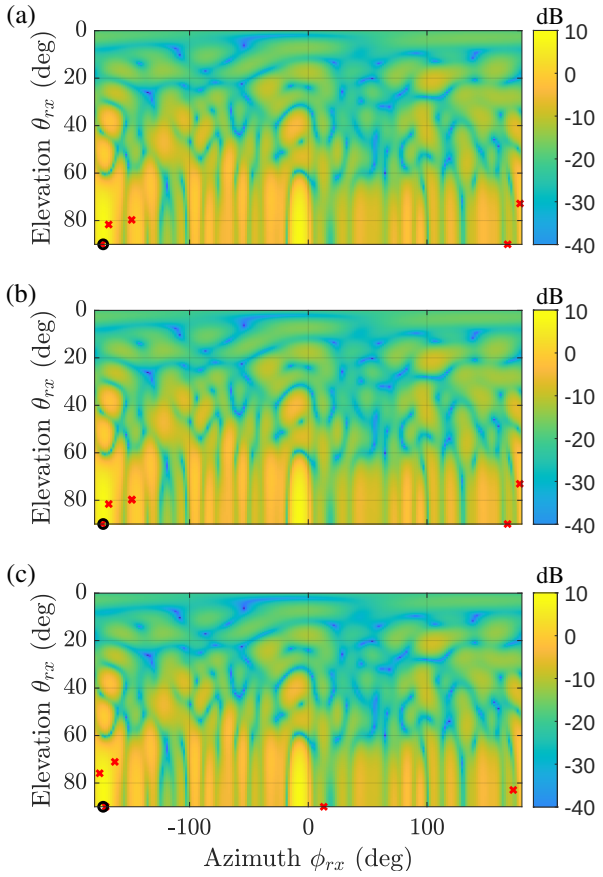

Fig. 5. DOAs corresponding to $\tilde{\mathbf{f}}_B$ as red crosses, conventional beamforming 19 at the receiver $P_{\text{RX,TX max}}$ as colored background, and maximum of 19 as black circle. (a) $\mu = 10$, (b) $\mu = 20$, and (c) $\mu = 200$. The direction of the transmit array is approximately at $\phi_{rx} = -180$ and θ_{rx} from the receiver array.

sparse approximated channel does not achieve a fit in terms of achievable rate.

C. Angular Information

From the Toeplitz matrices $\mathbf{T}_2(\mathbf{u})$ and $\mathbf{T}_2(\mathbf{v})$ the encoded frequencies $\mathbf{f}_{B,l}$ and $\mathbf{f}_{B,l}$ are retrieved and linked to DOA and direction of departure (DOD). A spatial periodogram is evaluated with respect to the receiver via conventional beamforming as

$$P_{\text{RX,TX max}} = |\mathbf{b}^H(\mathbf{f}_b)\mathbf{H}\mathbf{a}(\mathbf{f}_{a,l_{\text{TX max}}})|^2 \tag{19}$$

where $l_{\text{TX max}}$ is the transmit path with largest gain. The DOAs corresponding to the retrieved $\tilde{\mathbf{f}}_B \in [0,1)^{2\times K}$ at the indoor receiver are shown in Fig. 5. The agreement with the spatial receive periodogram $P_{\text{RX,TX max}}$ depends on the parameter μ. Whereas the largest peak is always recovered in the shown cases, the path around $\phi_{rx} = -180°$ and $\theta_{rx} = 90°$ is only recovered with higher μ. Additional DOAs are recovered near the largest peak of the periodogram with only small angular separation. The absence of a ground truth and the four-dimensional scenario renders the angular evaluation challenging.

IV. Conclusion

A sparse approximation of a measured outdoor-to-indoor massive MIMO channel was derived based on decoupled atomic norm minimization. The trade-off between sparsity and reconstruction quality is visible in the singular values of the approximation and the achievable rate. The strongest path according to a spatial receive periodogram is always recovered by the sparse approach. Additional paths are recovered with only small angular separation.

Acknowledgment

This work was supported by the 5G Internet of Things - Doctoral School. This work has been funded by the Christian Doppler Laboratory for Dependable Wireless Connectivity for the Society in Motion. The financial support by the Austrian Federal Ministry for Digital and Economic Affairs, the National Foundation for Research, Technology and Development and the Christian Doppler Research Association is gratefully acknowledged.

References

[1] E. Björnson, L. Sanguinetti, H. Wymeersch, J. Hoydis, and T. L. Marzetta, "Massive MIMO is a reality—what is next?: Five promising research directions for antenna arrays," *Digital Signal Processing*, vol. 94, pp. 3–20, 2019.

[2] X. Gao, O. Edfors, F. Rusek, and F. Tufvesson, "Massive MIMO performance evaluation based on measured propagation data," *IEEE Transactions on Wireless Communications*, vol. 14, no. 7, pp. 3899–3911, 2015.

[3] D. Schützenhöfer, S. Pratschner, H. Groll, and M. Rupp, "Channel rank analysis of an outdoor-to-indoor massive mimo measurement," in *2020 IEEE 21st International Workshop on Signal Processing Advances in Wireless Communications (SPAWC)*. IEEE, 2020, pp. 1–5.

[4] Stadt wien - viennagis - www.wien.gv.at/viennagis/.

[5] Y. Chi and M. Ferreira Da Costa, "Harnessing sparsity over the continuum: Atomic norm minimization for superresolution," *IEEE Signal Processing Magazine*, vol. 37, no. 2, p. 39–57, Mar 2020. [Online]. Available: http://dx.doi.org/10.1109/MSP.2019.2962209

[6] Z. Yang, J. Li, P. Stoica, and L. Xie, "Sparse methods for direction-of-arrival estimation," in *Academic Press Library in Signal Processing, Volume 7*. Elsevier, 2018, pp. 509–581.

[7] M. Wagner, Y. Park, and P. Gerstoft, "Gridless DOA estimation and root-music for non-uniform arrays," *arXiv preprint arXiv:2003.04457*, 2020.

[8] C. Steffens, M. Pesavento, and M. E. Pfetsch, "A compact formulation for the $\ell_{2,1}$ mixed-norm minimization problem," *IEEE Transactions on Signal Processing*, vol. 66, no. 6, pp. 1483–1497, 2018.

[9] Y. Tsai, L. Zheng, and X. Wang, "Millimeter-wave beamformed full-dimensional mimo channel estimation based on atomic norm minimization," *IEEE Transactions on Communications*, vol. 66, no. 12, pp. 6150–6163, 2018.

[10] H. L. Van Trees, *Optimum array processing: Part IV of detection, estimation, and modulation theory*. John Wiley & Sons, 2004.

[11] Z. Yang, L. Xie, and P. Stoica, "Vandermonde decomposition of multilevel toeplitz matrices with application to multidimensional super-resolution," *IEEE Transactions on Information Theory*, vol. 62, no. 6, pp. 3685–3701, 2016.

[12] Z. Tian, Z. Zhang, and Y. Wang, "Low-complexity optimization for two-dimensional direction-of-arrival estimation via decoupled atomic norm minimization," in *2017 IEEE International Conference on Acoustics, Speech and Signal Processing (ICASSP)*. IEEE, 2017, pp. 3071–3075.

[13] Z. Zhang, Y. Wang, and Z. Tian, "Efficient two-dimensional line spectrum estimation based on decoupled atomic norm minimization," *Signal Processing*, vol. 163, pp. 95–106, 2019.

[14] Y. Wang, P. Xu, and Z. Tian, "Efficient channel estimation for massive mimo systems via truncated two-dimensional atomic norm minimization," in *2017 IEEE International Conference on Communications (ICC)*. IEEE, 2017, pp. 1–6.